Organic & Biomolecular Chemistry

PAPER

View Article Online
View Journal | View Issue

Cite this: *Org. Biomol. Chem.*, 2017, **15**, 10105

Structure–reactivity correlations of the abnormal Beckmann reaction of dihydrolevoglucosenone oxime†

Amani Alhifthi,[a,b] Benjamin L. Harris,[a,b] Lars Goerigk,[a] Jonathan M. White *[a,b] and Spencer J. Williams *[a,b]

Received 10th October 2017,
Accepted 13th November 2017

DOI: 10.1039/c7ob02499a

rsc.li/obc

A structural, spectroscopic and computational study of a series of oximes was undertaken to investigate how geometric and structural changes relevant to the reaction coordinate for the Beckmann reaction (normal Beckmann) and Beckmann fragmentation (abnormal Beckmann) manifest in the ground state. X-ray structures of a range of oximes derived from dihydrolevoglucosan (Cyrene™; which undergoes the abnormal Beckmann reaction), in which the oxygen substituent was systematically varied were determined. As the electron demand of the OR group increased, the major structural changes included lengthening of the N–OR bond distance, and a decrease in the magnitude of the C2=N–O bond angle, consistent with the changes seen for cyclohexanone oximes, which undergo the normal Beckmann reaction. However, unique to the Cyrene oximes, an increase in the length of the fissile C1–C2 bond was observed, which correlated with a decrease in the ^{13}C–^{13}C 1-bond coupling constants as the electron demand of the OR substituent increased. Computational studies of Cyrene and cyclohexanone oximes using Natural Bond Orbital analysis support an electronic structure involving $n_{(O)} \rightarrow \sigma^*_{C1-C2}$ and $\sigma_{C1-C2} \rightarrow \sigma^*_{N-O}$ localized orbital interactions.

Introduction

Ketoximes undergo rearrangement reactions involving cleavage of the carbon–carbon bond adjacent to the imino carbon.[1] These reactions include the Beckmann rearrangement ('normal' Beckmann reaction),[2–4] leading to amides, and the Beckmann fragmentation ('abnormal' Beckmann reaction),[5,6] leading to nitriles. The normal Beckman reaction involves the generation of an incipient carbocation at the carbon atom located *anti* to the oxime oxygen, which is intercepted by migration to nitrogen to afford a nitrilium ion intermediate, which is subsequently hydrolyzed to yield an amide (Fig. 1). The abnormal Beckmann reaction occurs in cases where the adjacent carbon can stabilize positive charge; a carbocation intermediate is formed that undergoes heterolytic fragmentation of the carbon–carbon bond *anti* to the leaving group to yield a nitrile.[7–12] The initiating step of both the normal and abnormal Beckmann reactions involve the departure of an

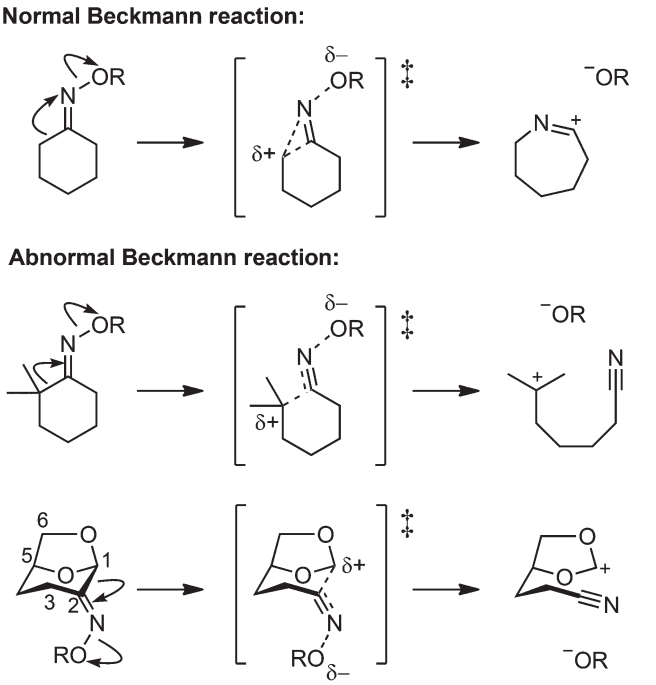

Fig. 1 Normal Beckmann (Beckmann rearrangement) and abnormal Beckmann (Beckmann fragmentation) reactions of oximes.

[a]*School of Chemistry, University of Melbourne, Parkville, Victoria, 3010, Australia. E-mail: sjwill@unimelb.edu.au, whitejm@unimelb.edu.au*
[b]*Bio21 Molecular Science and Biotechnology Institute, University of Melbourne, Parkville, Victoria, 3010, Australia*

† Electronic supplementary information (ESI) available. CCDC 1578343–1578350. For ESI and crystallographic data in CIF or other electronic format see DOI: 10.1039/c7ob02499a

oxygen leaving group from nitrogen, with the propensity of a substrate to undergo one or the other transformation dictated by the nature of the *anti* substituent.[13]

The structure-correlation principle emerged from early studies by Dunitz[14–16] and Kirby[17–19] who noted that for unimolecular reactions, changes in bond length and geometry at reactive sites in a molecule vary in a systematic manner that correlates with changes in reactivity of the substrate induced by varying its electronic nature. The structure-correlation principle can be applied in systems where the minimum energy (hereafter 'ground state') geometries are similar to that of the transition state. This allows application of the qualitative concept of frontier molecular orbital (FMO) interactions that facilitate the reaction to be manifested in the ground state. The structure-correlation principle is most readily applied by performing low temperature X-ray structures on substrates that are systematically varied to allow accurate measurement of geometric parameters, which are correlated with reactivity parameters such as leaving group ability. Structure–reactivity correlations of cyclohexanone oxime analogues that varied in the nature of the group OR revealed structural changes consistent with the manifestation of early stages of the normal Beckmann reaction.[20] These included an increasing N–OR bond distance and a closing of the N–C1–C2 bond angle, consistent with the early stages of bond breaking and of migration of the antiperiplanar carbon onto nitrogen. Additionally, the magnitude of the $^1J_{C-C}$ coupling constants for the migrating bond varied in a systematic way that supported meaningful changes in bond order consistent with the normal Beckmann reaction. A similar plot for the 2,2-dimethylcyclohexanone oxime analogues, which are prone to abnormal Beckmann reaction, revealed structural effects that varied in a similar fashion but which were weaker in magnitude.

In the present work we apply the structure-correlation principle to the abnormal Beckmann reaction for an oxime derivative bearing heteroatom donors on the *anti* carbon. We used the ketone dihydrolevoglucosenone (Cyrene™), which has recently become readily available on large scale through the valorization of wood-waste using the Furacell process.[21] Cyrene readily forms an oxime which undergoes the abnormal Beckmann reaction as a result of the effects of two donor oxygen atoms on the antiperiplanar carbon, causing a Grob fragmentation.[22] Moreover, the bicyclic nature of this compound provides a rigid structure that minimizes molecular flexibility while at the same time orienting the donor oxygens so as to provide effective orbital mixing in the ground state.

Results and discussion

Synthesis and structure-determinations of Cyrene-based oximes

A range of Cyrene-based oximes of varying leaving group ability (pK_a 16–2.85 for the conjugate acid) were synthesized. Reaction of Cyrene with $HONH_2{\cdot}HCl$ in pyridine afforded the parent oxime **1** as a single geometrical isomer,[22] a result which

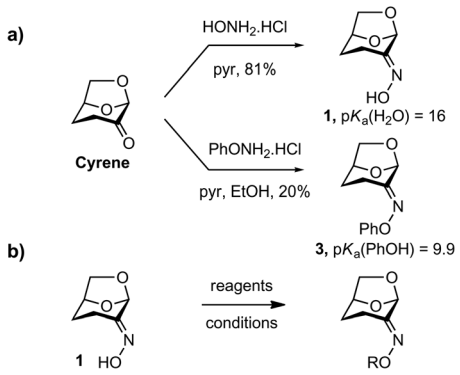

reagent	conditions	yield (%)	product	pK_a (ROH)
4-$BrC_6H_4CH_2Br$	NaH, DMF	78	**2**	14.2
4-$NO_2C_6H_4F$	NaH, THF	26	**4**	7.15
Ac_2O	pyr	61	**5**	4.75
3-NO_2-C_6H_4COCl	pyr, CH_2Cl_2	58	**6**	3.46
4-NO_2-C_6H_4COCl	pyr, CH_2Cl_2	52	**7**	3.44
3,5-$(NO_2)_2$-C_6H_3COCl	pyr, CH_2Cl_2	67	**8**	2.85

Fig. 2 Synthesis of Cyrene oxime and derivatives. (a) Condensation reactions for preparation of compounds **1** and **3**. (b) Acylation, arylation and alkylation reactions for preparation of compounds **2** and **4–8**. pK_a values are from ref. 23 and are for aqueous solutions.

reflects both steric as well as electronic effects (Fig. 2a). Alternatively, reaction of Cyrene under similar conditions with $PhONH_2{\cdot}HCl$ afforded the *O*-phenyl oxime **3**. A range of acylated and alkylated oximes of varying leaving group ability were prepared directly from **1** as shown in Fig. 2b. Thus alkylation or arylation using NaH in *N*,*N*-dimethylformamide (DMF) or tetrahydrofuran (THF) afforded **2** and **4**. Acylation with anhydrides or acyl halides in pyridine afforded **5–8**.

Oximes **1–8** were crystalline compounds and provided crystals suitable for single crystal X-ray structure determinations. The structures of oxime derivative **1–8** were determined at low temperature to minimise the effects of thermal libration on the measured geometric parameters. Representative thermal ellipsoid plots are shown in Fig. 3. In several cases unit cells contained non-equivalent structures ($Z' > 1$), which were treated as independent in subsequent analysis. Selected bond-distances and angles are presented in ESI Table S1.†

The ability of Cyrene-derived oximes to act as substrates for the abnormal Beckmann was investigated by refluxing a solution of oxime acetate **5** in acetic anhydride (Fig. 4). This led to the conversion to a mixture of nitriles **9** and **10**. While the volatility of the products led to their isolation in only modest yield, thin layer chromatography of the reaction mixture suggested that these were the only products to arise from the reaction and thus that abnormal Beckmann reaction is the major reaction channel. We also prepared and unsuccessfully attempted to obtain diffraction quality crystals of the 2-nitrobenzoyl oxime **11** (for 2-nitrobenzoic acid, $pK_a = 2.17$). Interestingly, a solution of **11** in $CDCl_3$ rearranged smoothly to a similar mixture of nitriles **12** and **13** upon storage at room temperature for 10 days.

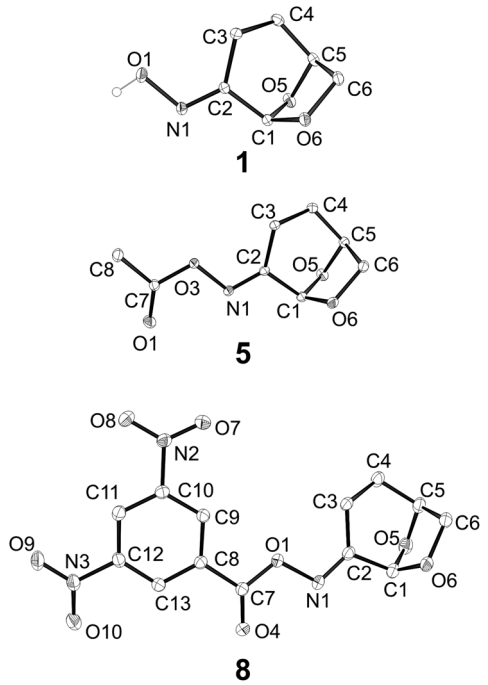

Fig. 3 Representative X-ray structures of oxime **1**, oxime acetate **5**, and 3,5-dinitrophenyloxime **8**.

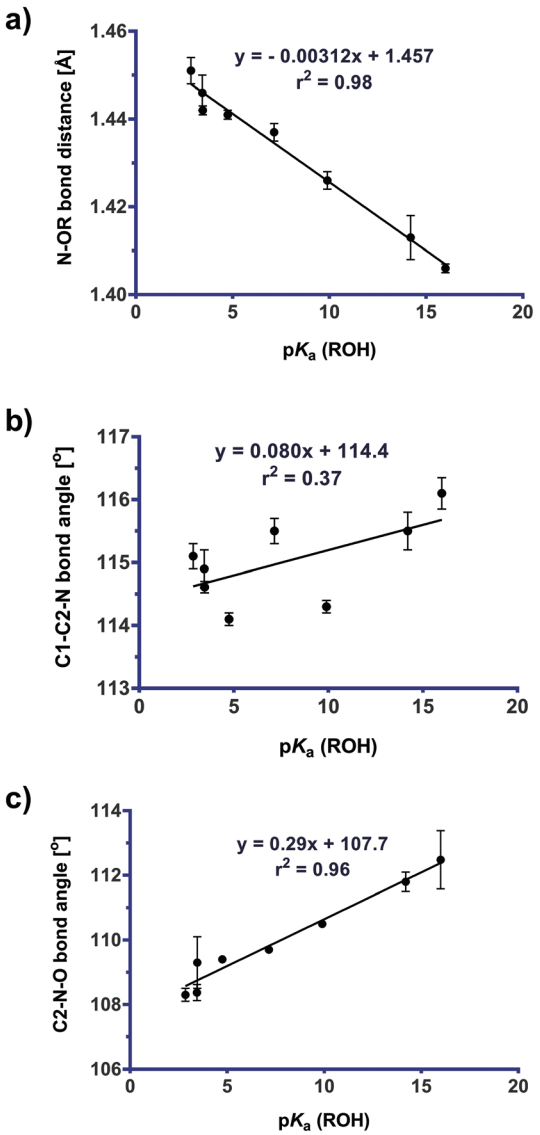

Fig. 5 Plot of (a) N–OR bond distance, (b) C1–C2–N bond angle [°], and (c) C2–N–O bond angle [°] *versus* pK_a (ROH) values for Cyrene oxime derivatives (**1–8**). See ESI Fig. S1† for a more comprehensive plot of critical bond distances and angles across this series.

Structural correlations in Cyrene oximes

The geometrical data obtained from the low temperature X-ray structures was used to construct the plots presented in Fig. 5. The data in Fig. 5a represents an application of the variable oxygen probe, with the slope exhibiting sensitivity to the nature of the leaving group. That is, as the leaving group ability increases (as quantified based on the pK_a value of the conjugate acid), the N–OR bond distance increases. This lengthening of the fissile bond can be taken to represent the early stages of the abnormal Beckmann reaction. Fig. 5b and c show the effects of the variable oxygen probe on the C1–C2–N and C2–N–O bond angles. These plots show that as leaving group ability increases, both bond angles decrease. Again, these changes can be interpreted as representing early stages of an abnormal Beckmann in which departure of the leaving group results in a change in hybridization at C2 and N from sp^2 to sp; this should lead to a contraction of the C1–C2–N angle (and a concomitant expansion of the C3–C2–N angle), and contraction of the C2–N–O angle reflecting the changing hybridisation of the N2 lone pair electrons from sp^2 towards sp and repulsion of the σ_{N-O} electrons (*vide infra*).

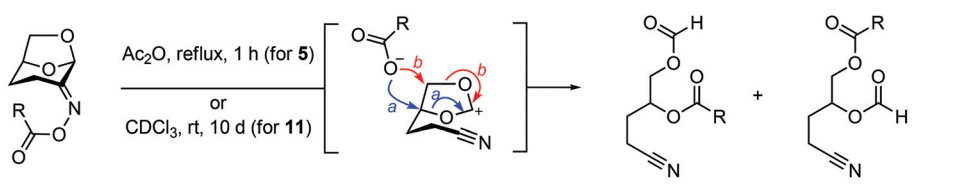

5 R = CH_3
11 R = 2-$NO_2C_6H_4$

9 R = CH_3
12 R = 2-$NO_2C_6H_4$

10 R = CH_3
13 R = 2-$NO_2C_6H_4$

Fig. 4 Abnormal Beckmann reactions of Cyrene oxime acetate **5** or 2-nitrobenzoate **11** affords a mixture of nitrile regioisomers. The stereochemistry was not determined.

From an FMO perspective, the observed geometric changes can be considered to arise from $\sigma_{C1-C2} \rightarrow \sigma^*_{N-O}$ interactions for the C1–C2 bond, which because of the presence of the two donor oxygens acts as a 'Grob-like' donor. Evidence for participation of the *anti* bond (C1–C2) in this interaction is illustrated in Fig. 6a in which the C1–C2 bond distance increases systematically with increasing leaving group ability of the OR substituent, while the C2–C3 bond (the *syn* bond) is essentially unchanged over the same series. Structure-correlation plots for the O5–C1 and O6–C1 bonds reveal a weak contraction of the bond distance as leaving group ability increases (Fig. 6b). The weakness of this correlation is presumably a consequence of distribution of structural effects over two bonds for the two donors, attenuating the structural consequences of electronic perturbation. Examination of the geometry of the X-ray structures reveals that O5, which is present within a tetrahydropyran ring, is geometrically disposed to provide better donation into the C1–C2 bond than O6, which is present within a tetrahydrofuran ring. An estimate for the angle of the donor lone pair can be obtained by using the AFIX 23 command within SHELXL2014,[24] which was used to place hydrogens on O5 and O6, enabling measurement of the dihedral angle for the C1–C2 bond of −168° for O5 and 150° for O6 for hypothetical sp^3 hybrid lone pair orbitals on each oxygen. This donor effect manifests within the X-ray structures as slightly shorter distances for the C1–O5 bonds compared to C1–O6, suggesting a stronger $n_{O5} \rightarrow \sigma^*_{C1-C2}$ interaction (*vide infra*).

One-bond ^{13}C–^{13}C coupling constants have been shown to be sensitive to the effects of hyperconjugation.[25] Further insight into $\sigma_{C1-C2} \rightarrow \sigma^*_{N-O}$ interactions in these structures, and their increasing magnitudes with leaving group ability is provided by the one-bond ^{13}C–^{13}C coupling constants, which were measured for selected derivatives. The one-bond ^{13}C–^{13}C coupling constants were determined using a 1D-INADEQUATE pulse sequence, or alternatively could be measured directly from the 1D ^1H decoupled ^{13}C NMR spectrum acquired for concentrated solutions. However, because of the poor sensitivity of these measurements, and the low solubility of several of the oxime derivatives (**4** and **6**), the coupling constants could only be obtained for six compounds (**1–3**, **5**, **7** and **8**). Fig. 7 shows that the $^1J_{C1-C2}$ coupling constant decreases with increasing leaving group ability of the OR group, which indicates a reduction in bond order, and is consistent with a greater $\sigma_{C1-C2} \rightarrow \sigma^*_{N-O}$ interaction across the series. Comparison of the line of least squares for that of a similar plot of cyclohexanone oximes ($y = 0.240x + 42.47$, $r^2 = 0.97$), with that determined here for the Cyrene oximes ($y = 0.33x + 56.09$, $r^2 = 0.87$), reveals that while they exhibit similar slopes, there is a striking difference in the *Y*-intercept, representing the expected coupling magnitude of C1–C2 for a leaving group with pK_a value of 0 for the conjugate acid, with the former some 14 Hz greater. This difference most likely reflects a fundamental mechanistic distinction of the normal and abnormal Beckmann reactions. In the normal Beckmann reaction, alkyl migration produces a partial positive charge on the oxime carbon, whereas in the abnormal Beckmann, the Grob-like fragmentation leads to positive charge development on the adjacent carbon (C1). ESI Fig. S2† shows the trend in ^{13}C chemical shift values for C1 and C2. C1 exhibits a decrease in chemical shift as a function of leaving group ability, while C2 exhibits an increase in chemical shift. Caution must be taken in the interpretation of these results as ^{13}C chemical shifts are sensitive to both electron demand and hybridization effects.

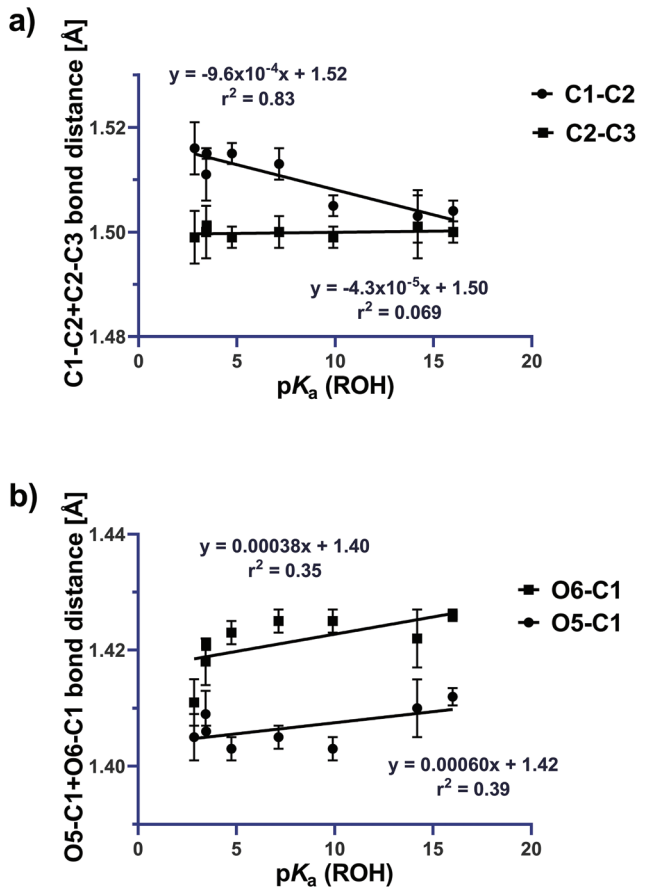

Fig. 6 Plots showing variations in (a) C1–C2 (*anti*) and C2–C3 (*syn*) bond distances and (b) O5–C1 and O6–C1 bond distances, as a function of leaving group ability.

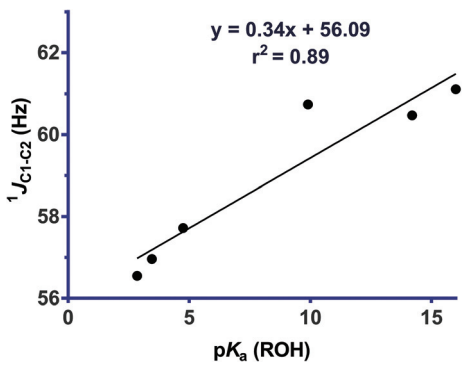

Fig. 7 Plot of $^1J_{C1-C2}$ for the antiperiplanar bond *versus* the pK_a (ROH) value for oxime derivatives **1–3**, **6–8**. The poor solubility of compounds **4** and **6** prevented measurement of their coupling constants.

We interpret the steep increase in C2 as arising primarily from the inductive effect of a better leaving group, while the weak decrease in C1 presumably reflects increased electron density at C1 from the donor oxygen atoms which is more than compensating for the decrease in electron density at C1 due to the $\sigma_{C1-C2} \rightarrow \sigma^*_{N-O}$ interaction.

The data presented here can be compared to published structure-correlation data for both the normal Beckmann reaction of cyclohexanone oximes, and the abnormal Beckmann reaction of 2,2-dimethylcyclohexanone oximes (Table 1). These data show that across the three series of compounds, the sensitivity of N–O bond length to increased leaving group ability is greatest for substrates that undergo the normal Beckmann reaction, with reduced sensitivity for substrates that undergo the abnormal Beckmann reaction, and especially the Cyrene oximes. This may reflect the increased ability of oxygen donors to support charge development at the remote site, leading to a reduced polarization of the C1–C2 bond. The sensitivity of the change in the N=C–C bond angle is greatest for the cyclohexanone series, and weakest for the two abnormal Beckmann series and especially the Cyrene oximes. In all three cases these angular structure–reactivity correlations reflect increasing sp character at the oxime carbon as the reaction progresses to a vinyl cation or nitrile (*vide infra*). These differences in sensitivity indicate that structural (and presumably electronic) rearrangements towards the azacyclopropene-like transition state of the normal Beckmann reaction occur earlier in the reaction coordinate, whereas the equivalent changes for the abnormal Beckmann reaction occur later. Finally, the sensitivity of the C=N–O bond angles are essentially the same for both reactions, indicating that departure of the leaving group occurs with similar timing and through a similar trajectory.

Electronic-structure correlations of normal and abnormal Beckmann reactions

Computational chemistry was used to provide qualitative insight into the electronic structure of the oximes and how this contributes to their propensity to undergo normal or abnormal Beckmann reactions. In particular, we sought to understand the key orbital interactions that contribute to their innate reactivity. We applied Natural Bond Orbital (NBO) analysis,[26,27] which transforms a given wave function or Kohn–Sham determinant from Density Functional Theory (DFT) into localized NBOs that represent lone pairs and covalent bonds commensurate with a traditional Lewis-type picture. For each bonding atom within a bond or lone pair, NBO data can be expressed in terms of percentage s, p and d character, or normalized relative to s character as a natural atomic hybrid (h_A). Departures from this localized Lewis-type structure through electron delocalization can subsequently be quantified using second order perturbation analysis. For each occupied Lewis-type donor NBO (i) and unoccupied non-Lewis-type acceptor NBO (j), the donor–acceptor stabilization energy $E(2)$ associated with $i \rightarrow j$ delocalization is calculated as:

$$E(2) = \Delta E_{ij}(2) = q_i F(i,j)^2/(\varepsilon_j - \varepsilon_i)$$

where q_i is the donor NBO occupancy (2 for closed-shell, 1 for open-shell), ε_i, ε_j are orbital energies, and $F(i,j)$ is the off-diagonal NBO Fock matrix element; see ref. 26 and 27 for more details. NBO analysis has proven an effective tool for the investigation of various hyperconjugative interactions in organic molecules.[28–30]

The geometries of a series of oximes derived from Cyrene and cyclohexanone of varying leaving group ability were optimized at the TPSS-D3(BJ)/def2-TZVP level of theory (see ESI†). The electronic structures of these models were then analyzed by NBO analysis at the hybrid-DFT PW6B95/def2-TZVP level of theory. Note that this DFT approximation has shown to be one of the most robust and reliable hybrids.[31] Table 2 shows that both systems exhibit $\sigma_{C1-C2} \rightarrow \sigma^*_{N-O}$ interactions, the magnitude of which, quantified by $E(2)$, increases as the electron demand of the variable oxygen probe increases. In a similar vein this data also shows that the occupancy of the σ_{C1-C2} donor orbital (q_i) decreases with increasing electron demand, which is consistent with these structures manifesting elec-

Table 1 Comparison of structure–reactivity correlations for ketone-derived oximes that undergo normal Beckmann reaction (cyclohexanone) and abnormal Beckmann reaction (2,2-dimethylcyclohexanone, Cyrene)

Series	r_{N-O} [Å]	r^2	Ref.
Cyclohexanone	$1.475 - (3.80 \times 10^{-3})$ pK_a (ROH)	0.86	20
2,2-Dimethylcyclohexanone	$1.467 - (3.20 \times 10^{-3})$ pK_a (ROH)	0.95	20
Cyrene	$1.457 - (3.12 \times 10^{-3})$ pK_a (ROH)	0.98	This work
Series	N=C–C [°]	r^2	Ref.
Cyclohexanone	$114.8 + (1.5 \times 10^{-1})$ pK_a (ROH)	0.67	20
2,2-Dimethylcyclohexanone	$115.4 + (1.37 \times 10^{-1})$ pK_a (ROH)	0.57	20
Cyrene	$114.4 + (0.80 \times 10^{-1})$ pK_a (ROH)	0.37	This work
Series	C=N–O [°]	r^2	Ref.
Cyclohexanone	$109.2 + (2.6 \times 10^{-1})$ pK_a (ROH)	0.68	20
2,2-Dimethylcyclohexanone	$108.7 + (2.8 \times 10^{-1})$ pK_a (ROH)	0.79	20
Cyrene	$107.7 + (2.9 \times 10^{-1})$ pK_a (ROH)	0.96	This work

Table 2 Donor–acceptor stabilization energies ($E(2)$) for $\sigma_{C1-C2} \rightarrow \sigma^*_{N-O}$ interactions in Cyrene and cyclohexanone oximes at the PW6B95/def2-TZVP level of theory. For natural atomic charges see Table S2

		Cyrene oximes			Cyclohexanone oximes		
R	pK_a	$E(2)$ (kcal mol^{-1})	ΔE_{ij} (au)	q_i	$E(2)$ (kcal mol^{-1})	ΔE_{ij} (au)	q_i
H	16	5.65	0.64	1.97376	5.60	0.61	1.97090
C_6H_5	9.9	6.00	0.64	1.97219	6.00	0.61	1.96928
CH_3CO	4.75	6.43	0.62	1.97017	6.34	0.59	1.96779
3-$NO_2C_6H_4CO$	3.46	6.53	0.61	1.96894	6.36	0.60	1.96759
3,5-$(NO_2)_2C_6H_3CO$	2.85	6.79	0.60	1.96750	6.60	0.59	1.96629
CF_3CO	0.50	7.20	0.59	1.96574	7.11	0.57	1.96344

tronic changes equivalent to early stages along the reaction coordinate for both abnormal and normal Beckmann reactions. A connection exists with the structure–reactivity correlations in which contractions of the C1–C2–N and C2–N–O angles provided qualitative evidence for a change in hybridization at C2 and N from sp^2 to sp. Across the series %s at N for the lone pair rises from 45.0 to 48.7 (h_A: $sp^{1.22}$ to $sp^{1.05}$), and % s at C2 for σ_{C2-C3} rises more modestly from 35.2 to 35.8 (h_A: $sp^{1.83}$ to $sp^{1.78}$) (Tables SI16 and SI17†). Simultaneously, the fissile bonds exhibit a reduction in s character at these two sites as the nucleofugacity of the leaving group OR increases; %s at N of the σ_{N-O} bond falls from 14.8 to 11.6 (h_A: $sp^{5.75}$ to $sp^{7.56}$), and %s at C2 for σ_{C1-C2} falls from 29.5 to 28.8 (h_A: $sp^{2.38}$ to $sp^{2.46}$) (Tables SI11 and SI15†).

NBO analysis was used to investigate the nature of remote donor effects by the endocyclic oxygens O5 and O6. The data in Table 3 reveals that donation by lone pairs on these remote oxygens increases as the leaving group ability increases, exhibiting the donor interactions necessary for the abnormal Beckmann reaction in the ground state for this system. While the X-ray structures suggest that O5, within the tetrahydropyran ring, is geometrically better disposed to act as a more effective donor than O6, within the tetrahydrofuran ring, NBO analysis does not provide evidence that the two oxygens are in fact significantly different in donor ability. To rule out any artefacts stemming from the chosen DFT approximation, extensive NBO calculations at five different levels of theory with the general gradient approximation (GGA) method revPBE, the meta-GGA TPSS, and the hybrid methods PW6B95, B3LYP, and PBE0 were conducted (see ESI Tables S3–10†). None of these provided clear evidence for superior donation by either oxygen.

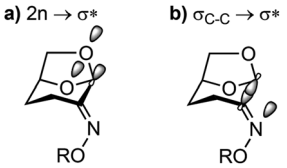

Fig. 8 Major orbital interactions in Cyrene oximes.

Conclusions

The structure–reactivity correlations of Cyrene oxime and derivatives show changes in bond-length and angles that are consistent with the early stages of the abnormal Beckmann reaction: lengthening of the fissile N–OR bond, and contraction of the C═N–O and C1–C2═N bond angles. More modest changes in the O5–C1 and O6–C1 bond distances are consistent with donor orbital contributions shared across these two donor atoms. While modest lengthening of the fissile C1–C2 bond distance was evident, more compelling evidence for electronic changes of this bond were revealed by measurement of one-bond ^{13}C–^{13}C coupling constants by NMR spectroscopy, indicating a reduction in electron density as leaving group ability increases. These experimental conclusions are supported by computational studies using NBO analysis, which revealed an increasing donor–acceptor stabilization energy $E(2)$, and a reduction in bond order (q_i), of the C1–C2 bond with increasing leaving group ability, and an increase in $n \rightarrow \sigma^*_{C1-C2}$ interactions of the adjacent oxygen donors. Collectively, the structural and electronic data are consistent with the major orbital interactions in the Cyrene oxime structures involving $n \rightarrow \sigma^*_{C1-C2}$ and $\sigma_{C1-C2} \rightarrow \sigma^*_{N-O}$ (Fig. 8).

Table 3 Donor–acceptor stabilization energies ($E(2)$) for $n_{O5} \rightarrow \sigma^*_{C1-C2}$ and $n_{O6} \rightarrow \sigma^*_{C1-C2}$ interactions for Cyrene oximes at the PW6B95/def2-TZVP level of theory. Data is for the single lone pair (LP) on each oxygen that provides the greatest stabilization energy

		LP O5			LP O6		
R	pK_a	$E(2)$ (kcal mol^{-1})	ΔE_{ij} (au)	q_i	$E(2)$ (kcal mol^{-1})	ΔE_{ij} (au)	q_i
H	16	3.30	0.75	1.90644	3.50	0.74	1.91418
C_6H_5	9.9	3.37	0.74	1.91333	3.54	0.74	1.83150
CH_3CO	4.75	3.45	0.74	1.90456	3.61	0.73	1.91275
3-$NO_2C_6H_4CO$	3.46	3.55	0.74	1.90366	3.64	0.73	1.91189
3,5-$(NO_2)_2C_6H_3CO$	2.85	3.62	0.73	1.90300	3.79	0.73	1.91114
CF_3CO	0.50	3.63	0.73	1.90239	3.79	0.73	1.91076

This work shows the interplay between structural and electronic reorganization in the ground state[32] and provides glimpses of the orbital and geometrical changes that occur upon O···N bond scission. We extend early observations of Kirby *et al.*[33,34] for the structure–reactivity correlations of oximes in the Beckmann rearrangement and more recent work by White *et al.*[20] describing structure–reactivity correlations for the abnormal Beckmann rearrangement of 2,2-dimethylcyclohexane oximes.[20] Broadly, the sensitivity of most of the Cyrene oxime correlations are similar to that for related plots of cyclohexanone oximes and 2,2-dimethylcyclohexanone oximes, which undergo normal and abnormal Beckmann reactions respectively. However, uniquely, the Cyrene oximes show a lengthening of the C1–C2 bond upon increased leaving group ability, and a greater magnitude of one-bond ^{13}C–^{13}C coupling constants, supporting divergence of mechanism for the normal and abnormal Beckmann reactions.

Experimental

Synthesis

Proton (^{1}H NMR, 400 or 600 MHz) and proton-decoupled carbon-13 (^{13}C NMR, 100 or 150 MHz) nuclear magnetic resonance spectra were obtained in deuterochloroform or acetone-d_6 with residual protonated solvent or solvent carbon signals as internal standards. Abbreviations for multiplicity are s, singlet; d, doublet; t, triplet; q, quartet; m, multiplet. Flash chromatography was carried out on silica gel 60 according to the procedure of Still *et al.*[35] Analytical thin layer chromatography (t.l.c.) was conducted on aluminium-backed 2 mm thick silica gel 60 F_{254} and chromatograms were visualized with UV light or ceric ammonium molybdate (Hanessian's stain). High resolution mass spectra (HRMS) were obtained using an ESI-TOF-MS; all samples were run using 0.1% formic acid. Dry CH_2Cl_2, THF, and Et_2O were obtained from a dry solvent apparatus (Glass Contour of SG Water, Nashua, USA) as per the procedure of Pangborn *et al.*[36] Dry DMF was dried over 4 Å molecular sieves, pyridine was dried over KOH. Pet. spirits refers to petroleum ether, boiling range 40–60 °C.

(*Z*)-Dihydrolevoglucosenone oxime (1). A solution of dihydrolevoglucosenone (Cyrene®, 7.8 ml, 76.1 mmol) and $NH_2OH{\cdot}HCl$ (12.0 g, 173 mmol) in anhydrous pyridine (100 mL) was stirred for 1.5 h. The reaction mixture was diluted with EtOAc (250 mL) and washed with H_2O (2 × 250 mL), aq. 1 M HCl (2 × 250 mL), sat. aq. $NaHCO_3$ (2 × 250 mL) and sat. aq. NaCl (2 × 250 mL). The organic layer was dried ($MgSO_4$) and concentrated under reduced pressure. The solid residue was recrystallized from 3 : 1 petroleum ether/EtOAc to afford the oxime **1** as white needles (8.85 g, 81%), mp = 104–110 °C; $[\alpha]_D^{20}$ −185.9 (*c* 0.7, $CHCl_3$; lit.[22] $[\alpha]_D^{20}$ −100.5); ^{1}H NMR (400 MHz, $CDCl_3$) δ 7.71 (1 H, s, OH), 5.52 (1 H, s, H1), 4.69–4.63 (1 H, m, H5), 3.93 (1 H, d, *J* = 7.2 Hz, H6), 3.88 (1 H, t, *J* = 5.7 Hz, H6′), 3.07 (1 H, dd, *J* = 16.9, 7.3 Hz, H3), 2.25 (1 H, ddd, *J* = 16.9, 11.6, 8.2 Hz, H3′), 2.13–2.01 (1 H, m, H4), 1.76 (1 H, dd, *J* = 13.8, 8.2 Hz, H4′); ^{13}C NMR (150 MHz, $CDCl_3$) δ 154.1 (C2), 100.2 (C1), 73.3 (C5), 67.0 (C6), 27.5 (C4), 16.0 (C3); IR (thin film) ν 689, 741, 883, 950, 1105, 1170, 1428, 1449, 2900, 3299 cm^{-1}.

(*Z*)-Dihydrolevoglucosenone *O*-(4-bromobenzyl)oxime (2). Sodium hydride (135 mg, 3.38 mmol) was added to a solution of oxime **1** (404 mg, 2.82 mmol) in DMF (12 mL). Next, a solution of 4-bromobenzyl bromide (838 mg, 3.38 mmol) in DMF (6 mL) was added to the reaction mixture. After 21 h the reaction mixture was diluted with Et_2O (30 ml) and washed with cold H_2O (3 × 50 ml). The organic layer was dried ($MgSO_4$) and concentrated under reduced pressure to give brown residue. Flash chromatography (EtOAc/pet. spirits 30 : 70) of the residue afforded a colourless solid, which was recrystallized from MeOH/pet. spirits to give compound **2** as white needles (685 mg, 78%), mp = 72–76 °C; $[\alpha]_D^{20}$ −82.6 (*c* 0.66, $CHCl_3$); ^{1}H NMR (400 MHz, $CDCl_3$) δ 7.47(2 H, app. d, *J* = 8.3 Hz, Ar), 7.20 (2 H, app. d, *J* = 8.2 Hz, Ar), 5.51 (1 H, s, H1), 5.00 (2 H, s, CH_2), 4.66–4.62 (1 H, m, H5), 3.91 (1 H, d, *J* = 7.0 Hz, H6), 3.87 (1 H, t, *J* = 6.2 Hz, H6′), 3.01 (1 H, dd, *J* = 17.0, 7.3 Hz, H3), 2.25 (1 H, ddd, *J* = 17.0, 11.5, 8.2 Hz, H3′), 2.09–2.00 (1 H, m, H4), 1.73 (1 H, dd, *J* = 14.1, 8.5 Hz, H4′); ^{13}C NMR (150 MHz, $CDCl_3$) δ 153.4 (C2), 100.2 (C1), 73.2 (C5), 67.2 (C6), 27.5 (C4), 16.7 (C3), 75.1 (**C**H_2Ar), 121.8, 129.7, 131.5, 136.6 (6 C, Ar); IR (thin film) ν 685, 722, 782, 797, 870, 885, 983, 1103, 1107, 1339, 1588, 2891, 2935, 2969 cm^{-1}.

(*Z*)-Dihydrolevoglucosenone *O*-(phenyl)oxime (3). A solution of Cyrene® (0.5 mL, 4.9 mmol) in anhydrous pyridine (1.5 mL) and EtOH (1 mL) was stirred and treated with $PhONH_2{\cdot}HCl$ (679.4 mg, 4.7 mmol). After 48 h the reaction mixture was evaporated to dryness and concentrated under reduced pressure. The solid residue was recrystallized from MeOH/CH_2Cl_2 to afford the oxime as white needles (222 mg, 20%), mp = 60–64 °C; $[\alpha]_D^{20}$ −114.5 (*c* 0.5, $CHCl_3$); ^{1}H NMR (600 MHz, $CDCl_3$) δ 7.21 (2 H, app. t, *J* = 7.9 Hz, Ph), 7.09 (2 H, app. d, *J* = 8.4 Hz, Ph), 6.93 (1 H, app. t, *J* = 7.0 Hz, Ph), 5.59 (1 H, s, H1), 4.53 (1 H, br s, H5), 3.82 (1 H, d, *J* = 7.3 Hz, H6), 3.76 (1 H, t, *J* = 6.3 Hz, H6′), 3.10 (1 H, dd, *J* = 17.1, 7.3 Hz, H3), 2.30 (1 H, ddd, *J* = 16.9, 11.6, 8.2 Hz, H3′), 2.01–1.93 (1 H, m, H4), 1.64 (1 H, dd, *J* = 13.9, 8.2 Hz, H4′); ^{13}C NMR (150 MHz, $CDCl_3$) δ 159.0 (C2), 156.1, 129.2, 122.3, 114.6 (6 C, Ar), 99.8 (C1), 73.2 (C5), 67.2 (C6), 27.4 (C4), 17.0 (C3); IR (thin film) ν 692, 752, 892, 924, 989, 1112, 1162, 1202, 1221, 1485, 1593, 2159 cm^{-1}.

(*Z*)-Dihydrolevoglucosenone *O*-(4-nitrophenyl)oxime (4). Sodium hydride (142 mg, 3.56 mmol) was added to a solution of oxime **1** (510 mg, 3.56 mmol) in THF (12 mL). Next, 4-fluoronitrobenzene (0.367 mL, 3.56 mmol) was added to the reaction mixture. After 24 h the reaction mixture was diluted with Et_2O (30 mL) and washed with cold H_2O (3 × 50 mL). The organic layer was dried ($MgSO_4$) and concentrated under reduced pressure to give a yellow residue. Flash chromatography (EtOAc/pet. spirits 30 : 70) of the residue afforded a solid that was recrystallized from CH_2Cl_2/Et_2O to give the oxime as beige blocks (250 mg, 26%), mp = 125–128 °C; $[\alpha]_D^{20}$ −116.6 (*c* 0.64, $CHCl_3$); ^{1}H NMR (400 MHz, $CDCl_3$) δ 8.21 (2 H, app. d, *J* = 9.3 Hz, Ar), 7.27 (2 H, app. d, *J* = 9.5 Hz, Ar), 5.70 (1 H, s, H1), 4.73 (1 H, br s, H5), 4.0 (1 H, d, *J* = 7.3 Hz, H6),

3.95 (1 H, t, J = 6.3 Hz, H6′), 3.24 (1 H, dd, J = 17.1, 7.2 Hz, H3), 2.48 (1 H, ddd, J = 17.1, 11.6, 8.3 Hz, H3′), 2.21–2.12 (1 H, m, H4), 1.86 (1 H, dd, J = 13.7, 8.5 Hz, H4′);^{13}C NMR (150 MHz, $CDCl_3$) δ 157.9 (C2), 142.5, 114.4, 125.6, 163.71 (6 C, Ar), 99.6 (C1), 73.2 (C5), 67.5 (C6), 27.7 (C4), 17.5 (C3); IR (thin film) ν 701, 749, 883, 1105, 1231, 1338, 1484, 1509, 1587, 1608, 1725, 2854, 2924 cm^{-1}.

(*Z*)-Dihydrolevoglucosenone *O*-(acetyl)oxime (5). A solution of oxime **1** (504 mg, 3.52 mmol) in CH_2Cl_2 (5 mL) and anhydrous pyridine (0.28 mL) was treated with acetic anhydride (0.33 mL, 3.52 mmol). After 24 h the reaction mixture was evaporated to dryness and concentrated under reduced pressure. The solid residue was recrystallized from 3 : 1 petroleum ether/EtOAc to afford compound **5** as white needles (400 mg, 61%), mp = 40–46 °C; $[\alpha]_D^{20}$ −292.7 (c 1.5, $CHCl_3$); ^{1}H NMR (400 MHz, $CDCl_3$) δ 5.71 (1 H, s, H1), 4.69 (1 H, br s, H5), 3.97 (1 H, d, J = 7.3 Hz, H6), 3.91 (1 H, t, J = 6.9 Hz, H6′), 3.06 (1 H, dd, J = 17.0, 7.2 Hz, H3), 2.39 (1 H, ddd, J = 17.0, 11.7, 8.2 Hz, H3′), 2.16–2.07 (1 H, m, H4), 1.181 (1 H, dd, J = 14.0, 8.2 Hz, H4′); ^{13}C NMR (150 MHz, d_6-acetone) δ 168.6 (CO), 159.7 (C2), 99.6 (C1), 73.1 (C5), 67.5 (C6), 27.7 (C4), 17.9 (C3), 19.5 (CH_3); IR (thin film) ν 677, 796, 864, 921, 966, 988, 1110, 1166, 1369, 1432, 1654, 1760, 2910, 2980 cm^{-1}.

(*Z*)-Dihydrolevoglucosenone *O*-(3-nitrobenzoyl)oxime (6). A solution of oxime **1** (400 mg, 2.79 mmol) and 3-nitrobenzoyl chloride (518 mg, 3.10 mmol) in CH_2Cl_2 (8 mL) and anhydrous pyridine (1.5 mL) was stirred for 1 h. The reaction mixture was then diluted with CH_2Cl_2 and washed with cold H_2O (2 × 30 mL), cold aq. 1 M HCl (2 × 30 mL), cold sat. aq. $NaHCO_3$ (2 × 30 mL) and concentrated under reduced pressure. The solid residue was recrystallized from 3 : 1 MeOH/CH_2Cl_2 to afford compound **6** as colorless blocks (471 mg, 58%), mp = 79–83 °C; $[\alpha]_D^{20}$ −135.2 (c 0.73, $CHCl_3$); ^{1}H NMR (400 MHz, $CDCl_3$) δ 8.82 (1 H, s, Ar), 8.46 (1 H, d, J = 8.2 Hz, Ar), 8.39 (1 H, d, J = 8.9 Hz, Ar), 7.70 (1 H, t, J = 8.0 Hz, Ar), 5.82 (1 H, s, H1), 4.74 (1 H, br s, H5), 4.01 (1 H, d, J = 7.4 Hz, H6), 3.95 (1 H, t, J = 6.3 Hz, H6′), 3.21 (1 H, dd, J = 17.0, 7.2 Hz, H3), 2.60 (1 H, ddd, J = 17.1, 11.6, 8.3 Hz, H3′), 2.26–2.15 (1 H, m, H4), 1.90 (1 H, dd, J = 13.7, 8.5 Hz, H4′); ^{13}C NMR (150 MHz, $CDCl_3$) δ 161.82, 161.78 (C2, CO), 148.3, 135.4, 130.5, 130.1, 127.9, 124.4 (6 C, Ar), 99.3 (C1), 73.2 (C5), 67.6 (C6), 27.7 (C4), 18.4 (C3); IR (thin film) ν 677, 795, 864, 890, 921, 966, 988, 1110, 1167, 1186, 1203, 1222, 1344, 1369, 1432, 1653, 1761, 2909, 2982 cm^{-1}.

(*Z*)-Dihydrolevoglucosenone *O*-(4-nitrobenzoyl)oxime (7). A solution of oxime **1** (100 mg, 0.698 mmol) and triethylamine (0.1 mL) in THF (5 mL) was stirred and treated with 4-nitrobenzoyl chloride (167 mg, 0.837 mmol). After 2 h the reaction mixture was diluted with EtOAc (25 mL) and washed with cold H_2O (2 × 25 mL). The organic layer was dried ($MgSO_4$) and concentrated under reduced pressure. The solid residue was recrystallized from 2 : 1 petroleum ether/EtOAc to afford compound **7** as pale yellow blocks (105 mg, 52%), mp = 119–123 °C; $[\alpha]_D^{20}$ −65.7 (c 0.25, $CHCl_3$); ^{1}H NMR (600 MHz, $CDCl_3$) δ 8.32 (2 H, app. d, J = 8.9 Hz, Ar), 8.22 (2 H, app. d, J = 8.9 Hz, Ar), 5.88 (1 H, s, H1), 4.75 (1 H, br s, H5), 4.00 (1 H, d, J = 7.3 Hz, H6), 3.96 (1 H, t, J = 6.2 Hz, H6′), 3.2 (1 H, dd, J = 17.0, 6.5 Hz, H3), 2.57 (1 H, ddd, J = 17.1, 11.6, 8.3 Hz, H3′), 2.2–2.1 (1 H, m, H4), 1.98 (1 H, dd, J = 13.8, 8.3 Hz, H4′); ^{13}C NMR (150 MHz, $CDCl_3$) δ 161.8, 161.6 (C2, CO), 150.7, 130.7, 134.3, 123.7 (6C, Ar), 99.3 (C1), 73.1 (C5), 67.6 (C6), 27.8 (C4), 18.3 (C3); IR (thin film) ν 659, 709, 864, 858, 961, 983, 1010, 1069, 1165, 1237, 1342, 1520, 1740, 1754, 2904, 2975, 3113 cm^{-1}.

(*Z*)-Dihydrolevoglucosenone *O*-(3,5-dinitrobenzoyl)oxime (8). A solution of oxime **1** (500 mg, 3.49 mmol) and anhydrous pyridine (6 mL) in CH_2Cl_2 (17 mL) was stirred and treated with 3,5-dinitrobenzoyl chloride (876 mg, 3.80 mmol). After 18 h the reaction mixture was diluted with CH_2Cl_2 (20 mL) and washed with cold H_2O (2 × 30 mL), cold aq. 1 M HCl (2 × 30 mL) and cold sat. aq. $NaHCO_3$ (2 × 30 mL). The organic layer was dried ($MgSO_4$) and concentrated under reduced pressure. The solid residue was recrystallized from 2 : 1 Et_2O/CH_2Cl_2 to afford compound **8** as white fine crystals (777 mg, 67%), mp = 73–77 °C; $[\alpha]_D^{20}$ −116.4 (c 0.56, $CHCl_3$); ^{1}H NMR (400 MHz, $CDCl_3$) δ 9.27 (1 H, app. d, J = 1.7 Hz, Ar), 9.15 (2 H, app. t, J = 3.4 Hz, Ar), 5.83 (1 H, s, H1), 4.77 (1 H, br s, H5), 4.03 (1 H, d, J = 7.5 Hz, H6), 3.97 (1 H, t, J = 7.2 Hz, H6′), 3.20 (1 H, dd, J = 17.0, 7.2 Hz, H3), 2.64 (1 H, ddd, J = 19.4, 10.6, 8.8 Hz, H3′), 2.29–2.18 (1 H, m, H4), 1.94 (1 H, dd, J = 14.0, 8.2 Hz, H4′); ^{13}C NMR (150 MHz, $CDCl_3$) δ 162.8, 159.8 (C2, CO), 148.8, 132.6, 129.8, 122.8 (6C, Ar), 99.1 (C1), 73.1 (C5), 67.7 (C6), 27.8 (C4), 18.5 (C3); IR (thin film) ν 716, 830, 870, 910, 920, 1074, 1094, 1110, 1133, 1183, 1250, 1345, 1416, 1471, 1540, 1597, 1630, 1705, 1757, 3094 cm^{-1}.

Nitriles 9 and 10. A solution of oxime **5** (300 mg, 0.617 mmol) in acetic anhydride (3 mL) was stirred under reflux for 1 h. The reaction mixture was concentrated under reduced pressure. Flash chromatography (Et_2O 100%) of the residue gave a mixture of the title compounds (90 mg, 30%); $[\alpha]_D^{20}$ −47.6 (c 0.7, $CHCl_3$).

Major compound: ^{1}H NMR (600 MHz, $CDCl_3$) δ 8.09 (1 H, s, OCOH), 5.28–5.24 (1 H, m, H5), 4.28 (1 H, dd, J = 12.1, 3.7, H6), 4.10 (1 H, dd, J = 12.3, 5.3 Hz, H′6), 2.44 (2 H, ddd, J = 11.7, 7.5, 4.1 Hz, H3), 2.07 (3 H, s, CH_3), 2.02 (2 H, t, J = 7.4 Hz, H4); ^{13}C NMR (151 MHz, $CDCl_3$) δ 170.4, 160.0, 118.4, 69.4, 63.8, 26.7, 20.6, 13.5.

Minor compound: ^{1}H NMR (600 MHz, $CDCl_3$) δ 8.06 (1 H, s, OCOH), 5.18–5.09 (1 H, m, H5), 4.37 (1 H, dd, J = 12.1, 3.7, H6), 4.17 (1 H, dd, J = 12.3, 5.3 Hz, H6′), 2.44 (2 H, ddd, J = 11.7, 7.5, 4.1 Hz, H3), 2.10 (3 H, s, CH_3), 2.02 (2 H, t, J = 7.4 Hz, H4); ^{13}C NMR (151 MHz, $CDCl_3$) δ 170.2, 160.2, 118.5, 69.5, 63.4, 26.7, 20.8, 13.6; HRMS (ESI)$^+$ m/z 203.1027 $[C_8H_{15}N_2O_4^+ (M + NH_4)^+$ requires 203.1026].

IR (thin film) ν 752.8, 1050, 1161, 1231.5, 1370, 1428.7, 1722.3, 2245.8, 2923.6.

Dihydrolevoglucosenone *O*-(2-nitrobenzoyl)oxime (11). A solution of oxime **1** (480 mg, 2.93 mmol) and 2-nitrobenzoyl chloride (0.39 mL, 2.93 mmol) in CH_2Cl_2 (8 mL) and anhydrous pyridine (1.7 mL) was stirred for 35 min at 0° C. The reaction mixture was then diluted with CH_2Cl_2 and washed with cold H_2O (2 × 30 mL), cold aq. 1 M HCl (2 × 30 mL), cold

sat. aq. $NaHCO_3$ (2 × 30 mL) and then dried ($MgSO_4$) and concentrated to afford the crude 2-nitrobenzoate as a brownish oil; ^{1}H NMR (400 MHz, $CDCl_3$) δ 7.98 (1 H, d, J = 7.9 Hz Ar), 7.77–7.67 (3 H, m, Ar), 5.70 (1 H, s, H1), 4.68 (1 H, br s, H5), 3.95 (1 H, d, J = 7.4 Hz, H6), 3.89 (1 H, t, J = 6.2 Hz, H6′), 2.94 (1 H, dd, J = 17.1, 7.2 Hz, H3), 2.40 (1 H, ddd, J = 17.1, 11.6, 8.3 Hz, H3′), 2.14–2.05 (1 H, m, H4), 1.79 (1 H, dd, J = 13.8, 8.1 Hz, H4′); ^{13}C NMR (150 MHz, $CDCl_3$) δ 161.5, 159.6 (C2, CO), 147.7, 133.4, 132.1, 130.3, 126.4, 124.3 (6 C, Ar), 99.2 (C1), 73.1 (C5), 67.5 (C6), 27.7 (C4), 18.0 (C3).

Nitriles 12 and 13. Rearrangement of a solution of 2-nitrobenzoate oxime in $CDCl_3$ upon storage at room temperature for 10 d. Major compound: ^{13}C NMR (101 MHz, $CDCl_3$) δ 168.9, 161.0, 161.0, 148.5, 132.7, 132.0, 130.1, 126.4, 123.7, 119.4, 67.7, 67.0, 28.7, 13.5.

Crystallography

Intensity data for **1–7** were collected with an Oxford Diffraction SuperNova CCD diffractometer using either Mo-Kα or Cu-Kα radiation, the temperature during all data collections was maintained at 130.0(1) using an Oxford Cryosystems cooling device. The data for **8** was collected on the MX1 beamline at the Australian Synchrotron at 100 K.[37] The structures were solved by direct methods and difference Fourier synthesis.[24] Thermal ellipsoid plots were generated using the program ORTEP-3[38] integrated within the WINGX suite of programs.[39]

Crystal data for 1. $C_6H_9NO_3$ M = 143.14, T = 130.0(2) K, λ = 0.71073 Å, orthorhombic, space group $P2_12_12_1$, a = 8.5061(2), b = 15.9215(4), c = 9.6417(2) Å, V = 1305.77(5) Å^3, Z = 8, Z' = 2, D_c = 1.456 Mg M^{-3}, μ(Mo-Kα) = 0.117 mm^{-1}, F(000) = 608, crystal size 0.66 × 0.56 × 0.44 mm. θ_{max} = 40.8°, 26 005 reflections measured, 7762 independent reflections (R_{int} = 0.034) the final R = 0.0408 [$I > 2\sigma(I)$, 6894 data] and w$R(F^2)$ = 0.1076 (all data) GOOF = 1.087. Absolute structure parameter 0.1(2). CCDC 1578343.†

Crystal data for 2. $C_{13}H_{14}BrNO_3$ M = 312.16, T = 130.0(2) K, λ = 0.71073 Å, monoclinic, space group $C2$, a = 19.6367(8), b = 6.2680(2), c = 20.8548(12) Å, β = 99.680(4)°, V = 2530.3(2) Å^3, Z = 8, Z' = 2 D_c = 1.639 Mg M^{-3}, μ(Mo-Kα) = 3.249 mm^{-1}, F(000) = 1264, crystal size 0.64 × 0.35 × 0.05 mm. θ_{max} = 36.61°, 17 227 reflections measured, 10 861 independent reflections (R_{int} = 0.0312) the final R = 0.0471 [$I > 2\sigma(I)$, 8361 data] and w$R(F^2)$ = 0.1228 (all data) GOOF = 1.049. Absolute structure parameter −0.027(7). CCDC 1578344.†

Crystal data for 3. $C_{12}H_{13}NO_3$ M = 219.23, T = 130.0(2) K, λ = 1.54184 Å, orthorhombic, space group $P2_12_12_1$, a = 5.9489(1), b = 8.1059(1), c = 22.3033(4) Å, V = 1075.49(3) Å^3, Z = 4, D_c = 1.354 Mg M^{-3}, μ(Cu-Kα) = 0.808 mm^{-1}, F(000) = 464, crystal size 0.37 × 0.29 × 0.13 mm. θ_{max} = 76.76°, 8000 reflections measured, 2254 independent reflections (R_{int} = 0.0166) the final R = 0.0285 [$I > 2\sigma(I)$, 2239 data] and w$R(F^2)$ = 0.0716 (all data) GOOF = 1.053. Absolute structure parameter 0.02(4). CCDC 1578345.†

Crystal data for 4. $C_{12}H_{12}N_2O_5$ M = 264.24, T = 130.0(2) K, λ = 1.54184 Å, orthorhombic, space group $P2_12_12_1$, a = 6.7738(2), b = 11.4773(3), c = 14.8982(4) Å, V = 1158.26(6) Å^3, Z = 4, D_c = 1.515 Mg M^{-3}, μ(Cu-Kα) = 1.020 mm^{-1}, F(000) = 392, crystal size 0.40 × 0.16 × 0.07 mm. θ_{max} = 76.97°, 6221 reflections measured, 2287 independent reflections (R_{int} = 0.0262) the final R = 0.0298 [$I > 2\sigma(I)$, 2133 data] and w$R(F^2)$ = 0.0803 (all data) GOOF = 1.068. Absolute structure parameter −0.17(14). CCDC 1578346.†

Crystal data for 5. $C_8H_{11}NO_4$ M = 185.18, T = 130.0(2) K, λ = 0.71073 Å, orthorhombic, space group $P2_12_12_1$, a = 5.6704(2), b = 15.6773(6), c = 9.7844(3) Å, V = 869.80(5) Å^3, Z = 4, D_c = 1.414 Mg M^{-3}, μ(Mo-Kα) = 0.114 mm^{-1}, F(000) = 392, crystal size 0.64 × 0.35 × 0.05 mm. θ_{max} = 36.34°, 11 018 reflections measured, 4053 independent reflections (R_{int} = 0.0256) the final R = 0.0395 [$I > 2\sigma(I)$, 3573 data] and w$R(F^2)$ = 0.1102 (all data) GOOF = 1.068. Absolute structure parameter −0.3(3). CCDC 1578348.†

Crystal data for 6. $C_{13}H_{12}N_2O_6$ M = 292.25, T = 130.0(2) K, λ = 0.71073 Å, orthorhombic, space group $P2_12_12_1$, a = 7.3112(2), b = 12.3133(3), c = 13.9596(3) Å, V = 1256.71(5) Å^3, Z = 4, D_c = 1.545 Mg M^{-3}, μ(Mo-Kα) = 0.124 mm^{-1}, F(000) = 608, crystal size 0.76 × 0.58 × 0.36 mm. θ_{max} = 40.93°, 23 600 reflections measured, 8050 independent reflections (R_{int} = 0.0271) the final R = 0.0379 [$I > 2\sigma(I)$, 7008 data] and w$R(F^2)$ = 0.1085 (all data) GOOF = 1.074. Absolute structure parameter 0.0(2). CCDC 1578347.†

Crystal data for 7. $C_{13}H_{12}N_2O_6$ M = 292.25, T = 130.0(2) K, λ = 0.71073 Å, monoclinic, space group $P2_1$, a = 11.6567(5), b = 12.4748(5), c = 17.6511(6) Å, 98.457(4)°, V = 2538.82(17) Å^3, Z = 8, Z' = 4 D_c = 1.414 Mg M^{-3}, μ(Mo-Kα) = 0.123 mm^{-1}, F(000) = 1216, crystal size 0.44 × 0.37 × 0.04 mm. θ_{max} = 29.99°, 23 391 reflections measured, 12 230 independent reflections (R_{int} = 0.0306) the final R = 0.0495 [$I > 2\sigma(I)$, 9425 data] and w$R(F^2)$ = 0.1225 (all data) GOOF = 1.022. Absolute structure parameter 0.1(6). CCDC 1578349.†

Crystal data for 8. $C_{13}H_{11}N_3O_8$ M = 337.25, T = 100.0(2) K, λ = 0.71073 Å, orthorhombic, space group $P2_12_12_1$, a = 6.2700(13), b = 9.4560(19), c = 23.600(5) Å, V = 1399.2(5) Å^3, Z = 4, D_c = 1.601 Mg M^{-3}, μ = 0.136 mm^{-1}, F(000) = 696, crystal size 0.05 × 0.04 × 0.03 mm. θ_{max} = 27.87°, 23 414 reflections measured, 3333 independent reflections (R_{int} = 0.0338) the final R = 0.0339 [$I > 2\sigma(I)$, 3118 data] and w$R(F^2)$ = 0.0906 (all data) GOOF = 1.080. Absolute structure parameter −0.1(2). CCDC 1578350.†

Computational methods

All geometry optimizations and single-point energy calculations were done using the ORCA 4.0.0 program.[40] Geometry optimizations of all structures were performed at the dispersion-corrected TPSS[41]-D3(BJ)[42,43]/def2-TZVP[44,45] level of theory together with the resolution of the identity approximation to the Coulomb integral evaluation (RI-J).[46] The ORCA numerical quadrature grid option "4" was chosen and a self-consistent-field (SCF) convergence criterion of $10^{-7}E_h$. After obtaining converged MOs in single-point calculations, NBO analyses were performed with the NBO6.0[47] program based on five different DFT approximations and the def2-TZVP basis set: PW6B95,[48] TPSS, revPBE,[49] B3LYP,[50,51] and PBE0.[52,53] These

DFT approximations were chosen either for their known accuracy (PW6B95, TPSS, revPBE) or their popularity (B3LYP, PBE0).[31] Note that an additive dispersion correction of the DFT-D3 type does not influence the MOs and their energies, hence usage of DFT-D3(BJ) was not necessary for this part of the analysis. The numerical quadrature grid and SCF convergence options in all single-point calculations were the same as for the geometry optimizations. All (meta-)GGA calculations were again carried out with the RI-J approximation.

Conflicts of interest

There are no conflicts to declare.

Acknowledgements

We thank the Australian Research Council (ARC) for financial support. SJW is an ARC-funded Future Fellow (FT130100103), and LG received support as an ARC DECRA Fellow (DE140100550). AA is grateful to Jazan University for financial support and thanks the Saudi Arabian Cultural Mission (SACM). LG is also grateful for generous allocation of computer time and technical support by The University of Melbourne, Melbourne Bioinformatics (project RA0005), and the National Computational Infrastructure Facility in Canberra through the National Computational Merit Allocation Scheme (project fk5). We thank Circa Group for a generous gift of Cyrene.

References

1 R. E. Gawley, *Org. React.*, 1988, **35**, 14–24.
2 E. Beckmann, *Ber.*, 1886, **19**, 988–993.
3 A. H. Blatt, *Chem. Rev.*, 1933, **12**, 215–260.
4 B. Jones, *Chem. Rev.*, 1944, **35**, 335–350.
5 O. Wallach, *Justus Liebigs Ann. Chem.*, 1899, **309**, 1–31.
6 C. A. Grob, *Angew. Chem., Int. Ed. Engl.*, 1969, **8**, 535–546.
7 A. F. Ferris, *J. Org. Chem.*, 1960, **25**, 12–18.
8 R. K. Hill, B. G. McKinnie, R. T. Conley, P. S. Darby, H. van Halbeek and E. M. Holt, *Tetrahedron*, 1988, **44**, 3405–3412.
9 H. Fujioka, H. Yamamoto, M. Miyazaki, T. Yamanaka, K. Takuma and Y. Kita, *Tetrahedron Lett.*, 1991, **32**, 5367–5368.
10 C. A. Grob, H. P. Fischer, H. Link and E. Renk, *Helv. Chim. Acta*, 1963, **46**, 1190–1206.
11 R. P. Bakale, M. A. Scialdone and C. R. Johnson, *J. Am. Chem. Soc.*, 1990, **112**, 6729–6731.
12 P. A. Petukhov and A. V. Tkachev, *Tetrahedron*, 1997, **53**, 2535–2550.
13 I. V. Alabugin, in *Stereoelectronic Effects*, John Wiley & Sons, Ltd, 2016, pp. 183–213, DOI: 10.1002/9781118906378.ch7.
14 H. B. Burgi, J. D. Dunitz, J. M. Lehn and G. Wipff, *Tetrahedron*, 1974, **30**, 1563–1572.
15 H. B. Burgi, J. D. Dunitz and E. Shefter, *J. Am. Chem. Soc.*, 1973, **95**, 5065–5067.
16 P. Murrayrust, H. B. Burgi and J. D. Dunitz, *J. Am. Chem. Soc.*, 1975, **97**, 921–922.
17 F. H. Allen and A. J. Kirby, *J. Am. Chem. Soc.*, 1984, **106**, 6197–6200.
18 A. J. Briggs, R. Glenn, P. G. Jones, A. J. Kirby and P. Ramaswamy, *J. Am. Chem. Soc.*, 1984, **106**, 6200–6206.
19 P. G. Jones and A. J. Kirby, *J. Am. Chem. Soc.*, 1984, **106**, 6207–6212.
20 S. D. Yeoh, B. L. Harris, T. J. Simons and J. M. White, *Aust. J. Chem.*, 2012, **65**, 905–917.
21 J. Sherwood, M. De bruyn, A. Constantinou, L. Moity, C. R. McElroy, T. J. Farmer, T. Duncan, W. Raverty, A. J. Hunt and J. H. Clark, *Chem. Commun.*, 2014, **50**, 9650–9652.
22 F. A. Valeev, E. V. Gorobets, I. P. Tsypysheva, G. S. Singizova, L. K. Kalimullina, M. G. Safarov, O. V. Shitikova and M. S. Miftakhov, *Chem. Nat. Compd.*, 2003, **39**, 563–568.
23 J. A. Dean, *Lange's Handbook of Chemistry*, McGraw-Hill Inc, New York, 1999.
24 G. Sheldrick, *Acta Crystallogr., Sect. C: Struct. Chem.*, 2015, **71**, 3–8.
25 G. R. Jones, S. Caldarelli and P. Vogel, *Helv. Chim. Acta*, 1997, **80**, 59–64.
26 J. P. Foster and F. Weinhold, *J. Am. Chem. Soc.*, 1980, **102**, 7211–7218.
27 E. D. Glendening, C. R. Landis and F. Weinhold, *Wiley Interdiscip. Rev.: Comput. Mol. Sci.*, 2012, **2**, 1–42.
28 I. V. Alabugin, K. M. Gilmore and P. W. Peterson, *Wiley Interdiscip. Rev.: Comput. Mol. Sci.*, 2011, **1**, 109–141.
29 I. V. Alabugin and M. Manoharan, *J. Org. Chem.*, 2004, **69**, 9011–9024.
30 I. V. Alabugin and T. A. Zeidan, *J. Am. Chem. Soc.*, 2002, **124**, 3175–3185.
31 (*a*) L. Goerigk and S. Grimme, *Phys. Chem. Chem. Phys.*, 2011, **13**, 6670–6688; (*b*) L. Goerigk, A. Hansen, C. Bauer, S. Ehrlich, A. Najibi and S. Grimme, *Phys. Chem. Chem. Phys.*, 2017, DOI: 10.1039/c7cp04913g.
32 I. V. Alabugin, S. Bresch and G. dos Passos Gomes, *J. Phys. Org. Chem.*, 2015, **28**, 147–162.
33 P. G. Jones, M. R. Edwards and A. J. Kirby, *Acta Crystallogr., Sect. C: Cryst. Struct. Commun.*, 1986, **42**, 1230–1232.
34 M. R. Edwards, A. J. Kirby, P. R. Raithby and P. G. Jones, *Acta Crystallogr., Sect. C: Cryst. Struct. Commun.*, 1987, **43**, 300–303.
35 W. C. Still, M. Kahn and A. M. Mitra, *J. Org. Chem.*, 1978, **43**, 2923–2925.
36 A. B. Pangborn, M. A. Giardello, R. H. Grubbs, R. K. Rosen and F. J. Timmers, *Organometallics*, 1996, **15**, 1518–1520.
37 N. P. Cowieson, D. Aragao, M. Clift, D. J. Ericsson, C. Gee, S. J. Harrop, N. Mudie, S. Panjikar, J. R. Price, A. Riboldi-Tunnicliffe, R. Williamson and T. Caradoc-Davies, *J. Synchrotron Radiat.*, 2015, **22**, 187–190.
38 L. J. Farrugia, *J. Appl. Crystallogr.*, 1997, **30**, 565.
39 L. J. Farrugia, *J. Appl. Crystallogr.*, 1999, **32**, 837–838.

40 F. Neese, *Wiley Interdiscip. Rev.: Comput. Mol. Sci.*, 2012, **2**, 73–78.
41 J. Tao, J. P. Perdew, V. N. Staroverov and G. E. Scuseria, *Phys. Rev. Lett.*, 2003, **91**, 146401.
42 S. Grimme, J. Antony, S. Ehrlich and H. Krieg, *J. Chem. Phys.*, 2010, **132**, 154104.
43 S. Grimme, S. Ehrlich and L. Goerigk, *J. Comput. Chem.*, 2011, **32**, 1456–1465.
44 F. Weigend, *Phys. Chem. Chem. Phys.*, 2006, **8**, 1057–1065.
45 F. Weigend and R. Ahlrichs, *Phys. Chem. Chem. Phys.*, 2005, **7**, 3297–3305.
46 K. Eichkorn, F. Weigend, O. Treutler and R. Ahlrichs, *Theor. Chem. Acc.*, 1997, **97**, 119–124.
47 E. D. Glendening, J. K. Badenhoop, A. E. Reed, J. E. Carpenter, J. A. Bohmann, C. M. Morales, C. R. Landis and F. Weinhold, NBO 6.0, 2013.
48 Y. Zhao and D. G. Truhlar, *J. Phys. Chem. A*, 2005, **109**, 5656–5667.
49 Y. Zhang and W. Yang, *Phys. Rev. Lett.*, 1998, **80**, 890–890.
50 A. D. Becke, *J. Chem. Phys.*, 1993, **98**, 5648–5652.
51 P. J. Stephens, F. J. Devlin, C. F. Chabalowski and M. J. Frisch, *J. Chem. Phys.*, 1994, **98**, 11623–11627.
52 C. Adamo and V. Barone, *J. Chem. Phys.*, 1999, **110**, 6158–6170.
53 M. Ernzerhof and G. E. Scuseria, *J. Chem. Phys.*, 1999, **110**, 5029–5036.